ISSN-1996-918X

Cross Mark

Pak. J. Anal. Environ. Chem. Vol. 25, No. 1 (2024) 99 – 112

http://doi.org/10.21743/pjaec/2024.06.10

Study of Fe_3O_4-NPs Coated with an Alcoholic Extract of *C. Spinosa* to Identify Appropriate IC_{50} HTC116 Cancer Cells

Majid A. Mohaisen*[1] and M.M. Sirhan[2]

[1]Department of Chemistry, College of Science, University of Anbar, Ramadi, Iraq.

[2]Department of Chemistry, College of Education for Pure Sciences, University of Anbar, Ramadi, Iraq.

*Corresponding Author Email: majid.a.m@uoanbar.edu.iq

Received 23 November 2023, Revised 23 January 2024, Accepted 24 April 2024

Abstract

In this study, *C. spinosa* was used to prepare Fe_3O_4 nanoparticles using green synthesis, and an alcoholic extract of *C. spinosa* was used to coat them. The resulting Fe_3O_4 nanocomposite showed high IC_{50} activity against HTC116 cancer cells. We characterized the prepared Fe_3O_4-NP powder for phase size, shape, crystallographic arrangement, chemical composition, and surface charge using TEM, FESEM, XRD, FTIR, and zeta potential. Zeta potential confirmed NP surface charges -18.9 mV for Fe_3O_4 and -25 mV for Fe_3O_4 coated alcoholic extract, whereas XRD confirmed crystal shapes, and the FTIR study, functional groups at 505, 378, and 555 cm^{-1} showed Fe-O linkages in A1 (alcoholic extract), A2 (Fe_3O_4, green synthesis), and A3 (alcoholic extract coated with Fe_3O_4). C. spinosa exhibited C=C stretching at 1539 and 1558 cm^{-1}, while functional groups A1, A2, and A3 observed C=O stretching at 1626, 1647, and 1743 cm^{-1}. The green synthesis had spherical aggregates with an average size of 24.6±5.7 nm, and the alcoholic extract-coated synthesis had 27.3±7.5 nm. This was true even though the NPs had a crystal structure. Then, TEM measured 8.9±2.26 and 11.2±6.8 nm Fe_3O_4-NP thicknesses. The XRD analysis of the Fe_3O_4-NPs were 7.72 and 8.9 nm, respectively. The study found that Fe_3O_4 nanocomposites had the best IC_{50} at 32.49 µg/mL and the highest average viability at 20 µg/mL in code C. Following it were code B at 64.24 4.73% with an IC_{50} of 52.32 g/mL and code A at 69.25 1.07% with an IC_{50} of 78.95 g/mL. Code C had the lowest cell viability for HDF at 20 µg/mL, at 75.27±7.90%, with an IC_{50} of 569.47 µg/mL. Codes B and A came in second and third, with IC_{50}s of 488.23 and 243.77 µg/mL, respectively, which was in line with what the literature said would happen. Following lengthy procedures, it may be a promising drug in the future.

Keywords: Fe_3O_4 green synthesis, *C. spinosa,* Alcoholic extract, Anticancer IC_{50}, (HTC 116)

Introduction

Medicinal plants have remained potent medications for the treatment of several illnesses in human beings [1]. Consequently, herbal treatments have gained popularity. As a result of improved medical technology and disease resistance; the side effects, failures, and other issues have reduced [2]. Recent research has demonstrated that plant extracts contain effective compounds, resulting in the use of herbal medicines [3]. Synthetic antioxidants have a greater propensity to induce adverse effects than those sourced from untamed or cultivated medicinal plants [4].There are over 700 species of *Capparaceae*, which are divided into 40–50 groups. The majority of individuals employed in the gardening and business sectors are obscure. The preponderance of clans resides in the Mediterranean and the United States, 15 species inhabit dry Africa.Their medicinal properties include those of antioxidants, bacteria, cancer, diabetes, microbes, and viruses. This herb has anti-arthritic and purifying properties [5,6]. Nanomaterials exhibit diverse physical and chemical characteristics because of their size, surface, interface, and quantum effects. Biology, medicine, and engineering use metals nanoparticles [7]. FeNPs destroy pathogens and clean organic, metal, and nonmetal ion-contaminated matrices [8]. In addition, AgNPs inhibit Gram-positive and Gram-negative bacterial action. FeNPs clean the dirty medium of organic debris metals, non-metals, and colours. Inhibit bacterial growth [9]. Biochemicalproductionof nanoparticle is increasing because of its safety and environmental friendliness [10]. Using physical, chemical, and biological processes, metallic nanoparticles can be produced. These methods are energy-intensive, involve hazardous solvents, and create waste. Production of metallic NPs must be carried out using green methods. For years, plants, algae, fungus, bacteria, and viruses have produced inexpensive, safe, energy-efficient metallic NPs [11]. Green synthesis is safer, cheaper, greener, and more sustainable than chemical and physical techniques. Biology's distinctive, hygienic, economical, and effective methods of synthesis are becoming increasingly popular. Recently studied biological systems include plant extracts that decrease metal ions and create NPs. Commercial nanostructures must be sized and shaped [12]. For NP characterisation, FE-SEM, TEM, and powder X-ray diffraction are crucial [13].

Leaves, vegetables, and roots contain phytochemicals that help plants survive and prevent illness. Plant extracts include primary and secondary components. Terpenoids, alkaloids, flavonoids, and phenolics are secondary to chlorophyll, proteins, and carbohydrates [14]. The use of NPs improves chemotherapy. Gene therapy, NP-based hyperthermia, and tailored pharmaceutical administration may treat cancer without adverse effects. Effective gene-protecting drugs may also work. Nanomedicines, which are two times smaller than cancer cells, cannot interact with organelles and proteins. Nanomaterials may help cancerbecause it is possible to reduce harm to healthy tissues by designing nanoparticles that specifically target cancer cells [15]. Iron oxide is an attractive metal for NPs because it has several biological functions and is cheap and plentiful. Thus, it may compete for NPs. Nanomedicine can build non-toxic treatments and minimize drug-resistant bacterial strains by understanding NPs. With the right knowledge of NPs, nanomedicine can develop safe treatments and reduce the number of bacteria resistant to drugs. By producing and characterizing Fe3O4 nanoparticles sustainably, we will be able to identify the optimal IC50 value for use against cancer cell lines. To achieve our objective of creating a nanocomposite by coating it with an alcoholic extract.

Materials and Methods

Plant Material

The leaves of *C. spinosa*plants were gathered in 2022 from the El Baghdadi region of Anbar, Iraq, specifically during active growth (May/June). The Centre for Desert Studies at the University of Anbar categorized the fauna. Before drying in the shade at laboratory temperature, the plants were thoroughly cleaned and dried until they reached a consistent weight. Subsequently, they were stored in opaque containers and sealed until use.

Chemicals and Reagents

Iron (III) nitrate hexahydrate (Fe $(NO_3)_2$. $6H_2O$), Iron (III) chloridehexahydrate ($FeCl_3.6H_2O$), and Iron (II) chloride tetra hydrate ($FeCl_2.4H_2O$), phosphate-buffered saline (PBS) (Sigma- Aldrich), sodium hydroxide (NaOH), absolute ethanol, 60% ethanol, 3% H_2SO_4 solution (BDH), 25% NH_4OH (Fluka), dimethyl sulphide(µL), Dulbecco's modified Eagle medium (DMEM), and Dimethyl sulfoxide (DMSO) from Sigma- Aldrich, 5% fetal bovine serum, 3(4.5-dimethyl - thiazole-2-yl) 2,5-diphenyl tetrazolium bromide (MTT) from Thermo Fisher Scientific's.

Preparation of the Extracts from C.spinosa

After collection of the plant, it was washed with deionized water and allowed to dry in shade followed by grinding it into powder. Added 10 g of powder to a beaker and mixed with 200 mL of deionized water using a magnetic stirrer. Heated the mixture at 80°C for 30 min to obtain the brown extract, and then let it cool. Fig. 1 shows the filtered solution. The plant extract was concentrated in a glass vial at room temperature [16].

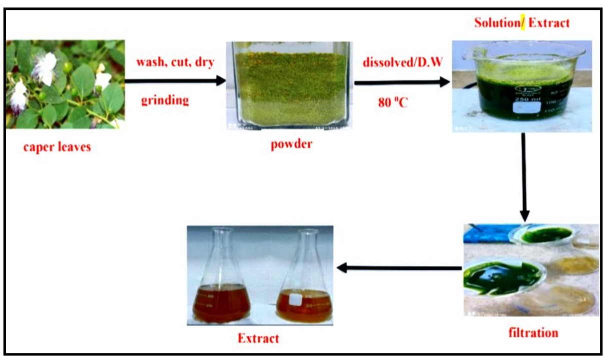

Figure 1. **Schematic diagram of preparation of the plant extract**

Alcoholic Extract (EE)

The extraction was carried out in accordance with the procedure outlined by Zhou *et al*., in which 10 g of *capers* powder was extracted three times for a total of 2 h using 100 mL of 60% ethanol concentration. The process was achieved using a magnetic stirrer for 2 h each time. The concentrated extract was concentrated in a rotary evaporator at 50 °C until the volume reached 20 mL. The filtrate was collected, and the concentrated extract was transferred onto a Petri dish and dried in an electric oven at 40 °C for 24 h. Then, place the clean, dry bottles with the dried powder inside the refrigerator until needed. [17].

Green synthesis of Fe_3O_4-NPs

This synthesis was conducted with minor adjustments as previously documented [16]. In summary, 2.2g of Fe $(NO_3)_2$. $6H_2O$ was introduced into 200 mL of deionized water in a 500mL beaker under magnetic stirring. Next, 20 mL of the plant extract was prepared as Figure 1. This volume was added gradually while stirring continuously at 25 °C using a burette containing drops, and the temperature was increased to 80 °C. The pH of the solution was adjusted by adding 1 M NaOH, which resulted in the formation of a brown precipitate, as illustrated in Fig. 2.

Allowed the precipitate to cool to room temperature and centrifuged at 1,200 rpm for 10 min to remove any residual fibers. Finally, the solution was filtered through a filter paper.

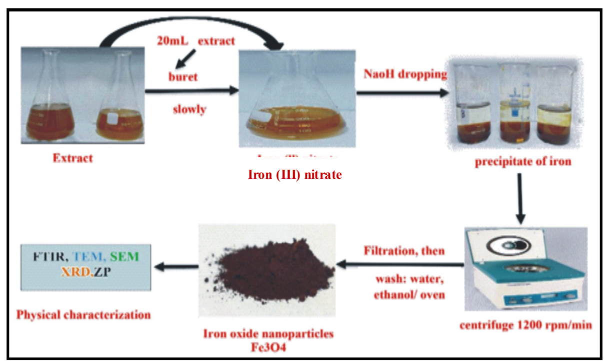

Figure 2. **Schematic diagram ofgreen synthesis of Fe_3O_4-NPsof *Capparis Spinosa***

Preparation of Fe_3O_4 Nanocomposite

Employed the co-precipitation technique, albeit with minor adjustments [18] to fabricate composites comprising Fe_3O_4-NPs coated with *C. spinosa* extracts (CEs). Initial dissolution of 1 g of CEs and 0.5 g of Fe_3O_4-NPs in 50 mL of deionized water in a beaker. An increase in the pH solution to 10 resulted in their rapid addition to the mélange. After concurrent addition, 24 h of churning at room temperature ensued. The resultant compound, Fe_3O_4-CEs, was gathered through the utilisation of a magnet after its dispersion under ultrasonic conditions. Following thorough washing with deionized water, the sample was desiccated at room temperature in a vacuum desiccator. The synthesis of Fe_3O_4 with different methods is mentioned with their code in Table 1.

Table 1. **Name of sample used in this study.**

Codes	Name of sample
A1	Alcoholic extract
A2	Fe_3O_4 (green synthesis), of C. spinosa
A3	Fe_3O_4- coated alcoholic extract

Evaluation of Anti-cancer Activity

The HCT116 colon and HDF cell lines were acquired from the Pasteur Institute in Tehran, Iran. The anticancer effects of the synthesised composites of Fe_3O_4-NP CEs were tested, and the median inhibitory dose IC_{50} for two different cancer cell lines was determined. Each cell suspension was harvested at a concentration of 5 x 104 cells per well on a 96-well flat-bottom plate containing DME) with 5% fetal bovine serum to measure its cytotoxicity. The Fe_3O_4–NP–CE synthesized composite was seeded at 20, 10, 5, 2.5, and 1.25 μg/mL. The plate was then incubated at 37°C with 5% CO_2 for 24 h.

After rinsing with a serum-free medium containing 100 μL of 5 mg/mL of MTT, the cells were grown for 4–5 h. After incubation, the cells were washed again with PBS. After solubilizing the unbound formazan with 100 μL of DMSO, the plates were measured at 570 nm using a Biotek (USA) plate reader. The formazan dye's color intensity was directly related to the number of live cells; hence, the optimal IC_{50} was obtained in triplicate [19].

Characterization of Fe_3O_4-NPs

Iron oxide nanoparticles, also known as Fe_3O_4-NPs, have been prepared using various techniques,one of which is a green synthesis that uses the leaves of *C. spinosa*. The surface charge, shape, and nanosize can be easily determined using various characterization techniques. The IR-Prestige-21 Shimadzu FTIR spectrophotometer demonstrated clear absorption bands on Fe_3O_4-NPs, confirming their production. FTIR records the IR absorption spectra at 400–4000 cm^{-1} [20].X-ray diffraction (XRD) was used to observe the crystalline structure and crystallinity of the NPs. Transmission electron microscopy (TEM) was used to observe the size and shape of the synthesised NPs at an accelerating voltage of 200 kV. TEM images of biosynthesised NPs and field emission scanning electron microscopy (FESEM) are imaging techniques used to analyze morphology and topography. In addition, the zeta potential (ZP) can be employed to determine the surface charge of NPs suspended in a liquid medium. The charged particle's surface exhibits an attractive force that facilitates the formation of a closely adhered layer of opposite charge, resulting in the creation of a narrow liquid layer referred to as the Stern layer [21].

Result and Discussion

FTIR Spectral Analysis

The KBr disc procedure was chosen for the analysis, as shown in Fig. 3 of the spectrum of the Fe_3O_4-NPs synthesis using green synthesis. These spectra visually represent the different processes involved in each synthesis technique. The FTIR spectra of Fe_3O_4-NPs extract may be used to determine the distinctive peaks of Fe_3O_4-NPs[22].The FTIR spectra of the green synthesized Fe_3O_4-NPs are shown in Fig. 3. The peaks in the FTIR spectrum that emerge in Fig. 3 between 3437, 3421, and 3217 cm^{-1}, which are linked to the phenolic molecule in the plant extract that is involved in the production of NPs, are due to the stretching vibration of the hydroxyl group (O-H) [23].

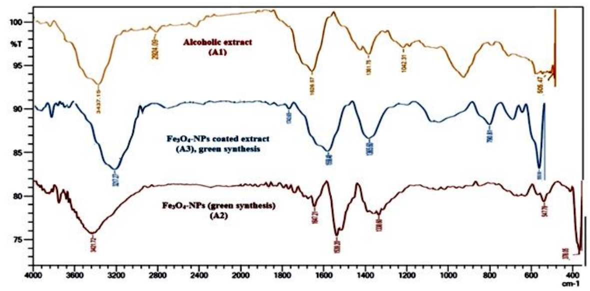

Figure 3. **FTIR image (A1) alcoholic extract (A2) Fe_3O_4-NPs (green synthesis) (A3) Fe_3O_4-NPs-coated alcoholic extract**

The stretching bands of the (C=C) 1539, 1558, and (C=O) 1626, 1647, and 1743 cm^{-1} in the (A1, A2, and A3) functional groups, respectively. The functional groups at 1626, 1647, and 1743 cm^{-1} in Fe_3O_4-NPs are probably attributed to the organic building blocks employed during synthesis. Fig. 3 shows basic absorption bands for the Fe-O bonds at 505, 378, and 555 cm^{-1} [24]. These absorption bands show that the crystal structure of the Fe_3O_4-NPs is well-characterized. Also, these distinct IR absorption bands are indicative of the Fe-O bonds at both the tetrahedral and octahedral positions, further supporting the pure Fe_3O_4-NPs spinel structure [25]. The spectra of magnetite NPs synthesised using green techniques and those coated with *C. spinosa* extracts show the formation of four unique bands at 1361, 1539, and 1558 cm^{-1} for (A1, A2, and A3), respectively. The asymmetric and symmetric stretching vibrations of the carboxyl group (COO) are responsible for these bands. The asymmetric and symmetric stretching vibrations of the CH_2 groups included in the coating agents are responsible for the bands seen at wavenumbers 2924, 2966, and 2989 cm^{-1} [26]. As a result of esterification between the carboxyl group of the acid molecule and the hydroxyl groups on the surface of the magnetite NPs, the four new bands indicate that the coating agents are bonded to the magnetite NPs.

Transmission Electron Microscopy

Transmission electron microscopy (TEM) with an accelerating voltage of 200 kV was used to determine the shape and size of the Fe_3O_4-NPs. The reaction solution was diluted with deionized water and sonicated for 10 min. The sonicated sample was drop-coated on carbon-coated copper grids and vacuum-dried for 30 min, and electron micrographs were taken. Understanding the morphology and size distribution of NPs is crucial for determining their properties and potential applications in various fields, such as medicine, electronics, and environmental science. Fig. 4 (A and B) shows the TEM image and the size distribution, respectively. Fig. A, which depicts the manufacture of Fe_3O_4-NPs from*C. spinosa* using green synthesis, makes it abundantly evident that the sizes of the Fe_3O_4-NPs were virtually consistent. Nevertheless, there are some aggregates in various sections of this sample. Furthermore, all particles were spherical and cubic. In addition, the particle size distribution curve of the Fe_3O_4-NPs revealed that the mean diameter of this NP was approximately 8.9 nm, with a standard deviation of 2.26. However, when the Fe_3O_4-NPs were coated with alcoholic extracts of *C. spinosa*, we detected a modest change in shape and size dispersion. This finding is in excellent agreement with the earlier FTIR data shown in Fig. 1. The average size of the Fe_3O_4-NPs coated in green synthesis was 11.2 nm, with a standard deviation of 3.2 in Fig. 4 (B)[27]. It was further established using TEM micrographs and the image-editing software ImageJ that the particle size increased following coating with *C. spinosa* extract [28]. Fe_3O_4 NPs coated with an extract from *spinosa* using green synthesis are shown in Table 2.

Table 2. **Size of Fe_3O_4-NPs green synthesis and coated alcoholic extract of *C. spinosa*.**

Type of samples	Average	St.dv.	Minimum	Medium	Maximum
Fe_3O_4-NPs green synthesis	8.9 nm	2.26	4.10	9.17	14.5
Fe_3O_4-coated alcoholic extract of C. spinosa	11.2 nm	3.2	6.3	10.5	22.5

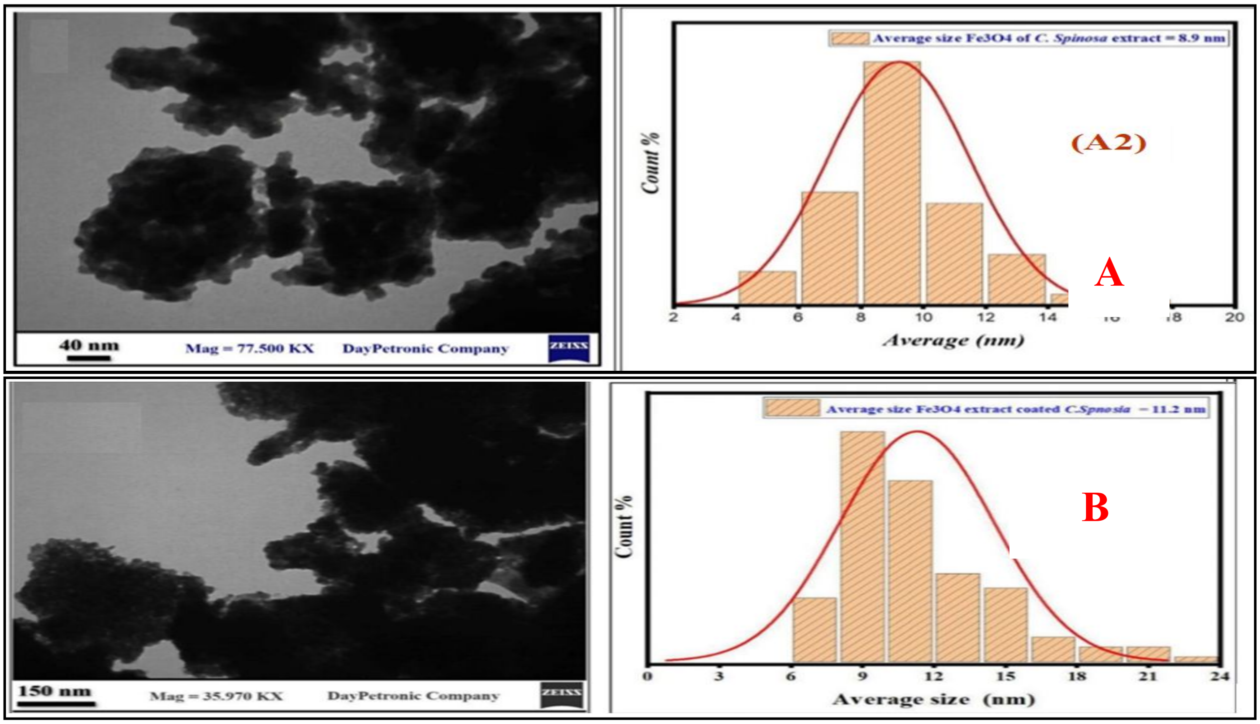

Figure 4. **TEM images of (A) Fe_3O_4-NPs green synthesis using *C. spinosa*(B) Fe_3O_4-NPs- coated alcoholic extract of *C. spinosa***

Field emission scanningelectron microscopy

Fe_3O_4-NPs were examined by FESEM. A very small amount of the sample was deposited on a carbon-coated copper matrix to create a thin film. The excess solution was removed using blotting paper, and the film on the FESEM grid was allowed to dry under a mercury lamp for 5 min. High-resolution imaging was used to study the structural characteristics. The FESEM analysis showed that the manufactured Fe_3O_4-NPs were almost spherical and monodispersed in shape. Fe_3O_4-NPs have a nearly spherical shape, which is critical for their magnetic characteristics and applications because it shows that the nanoparticles have a homogeneous size and shape [29].The Fe_3O_4-NPs that were artificially produced had an average size of 24.6 nm and 25.04 nm, respectively, as shown in Fig. 5 (A and B). The manufactured Fe_3O_4-NPs were evenly spread out and had a shape that was almost spherical when examined with FESEM [30].Nearly all the manufactured Fe_3O_4-NPs seemed to be perfectly spherical and were measured to be in the nm range. Green synthesis of Fe_3O_4-NPs and Fe_3O_4-NP-coated with an alcoholic extract of *C. spinosa* exhibited an increase in the size of Fe_3O_4-NPs, in agreement with the results obtained using FTIR and TEM. Overall, the almost spherical form of Fe_3O_4-NPs is important for their magnetic characteristics and applications, and it may be adjusted using several synthesis techniques, with more interpretation in Table 3.

Table 3. **Size of Fe_3O_4-NPs green synthesis and coated alcoholic extract of *C. spinosa.***

Type of samples (FESEM)	Average	St.dv.	Minimum	Medium	Maximum
Fe_3O_4-NPs (green synthesis)	24.6 nm	5.7	9.9	25.3	41.3
Fe_3O_4-NPscoated alcoholic extract of C. spinosa	27.3 nm	7.5	11.5	26.7	50.5

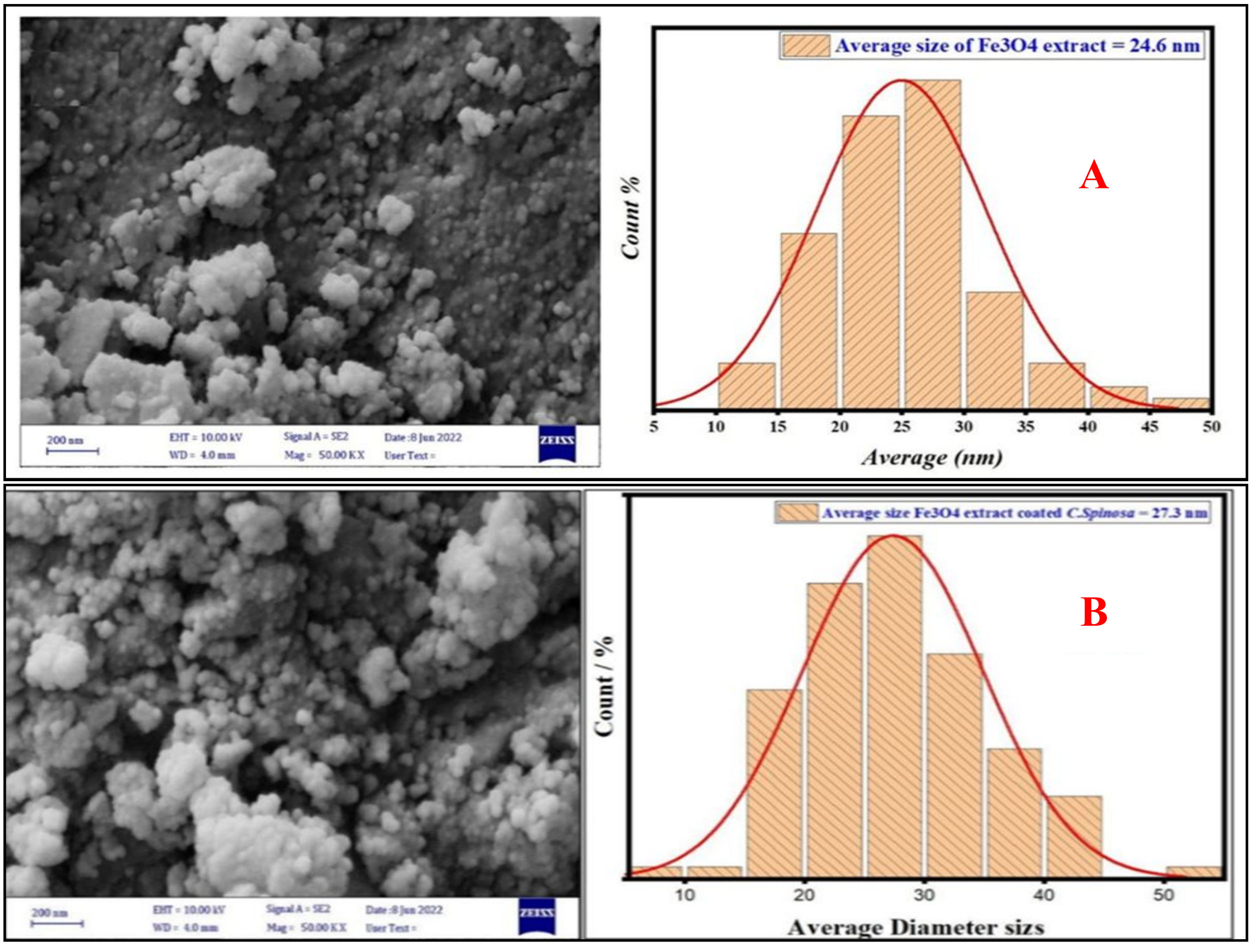

Figure 5.**FESEM image (A) Fe_3O_4-NPs green synthesis from *C. spinosa* (B) image Fe_3O_4-NPs- coated alcoholic extract of *C. spinosa***

X-ray diffraction (XRD) analysis

XRD is a non-destructive method for identifying crystalline materials and characterization of nanoparticle structures [31].It is used for measuring crystalline percentages and identifying fine spark minerals like NPs and nano clays. It has been used to characterize various metal NPs, including hematite, maghemite, and magnetite, using the Scherrer equation for average crystallite size determination [32].

Where d is the particle size, k is the Scherrer constant (0.9), is the X-ray wavelength (0.15406 nm), β is the width of the XRD peak at half-height, and θ is the Bragg diffraction angle. Fig. 6 (A and B) shows the X-ray diffraction patterns for the Fe_3O_4-NPs synthesized by green synthesisfrom *C. spinosa* [33]. It has been observed that there exist prominent diffraction peaks characterized by 2θ values of 30.3°, 35.6°, 43.3°, 53.9°, 57.3°, 62.9°, and 74.5°. These crystal planes reveal the precise arrangement of atoms within the structure of Fe_3O_4-NPs for these methods.

The (220), (311), (400), (422), (511), (440), and (533) planes are instrumental in determining the physical and chemical properties of NPs[34]. The findings demonstrate that the magnetite NPs possess a spinel phase structure, which aligns with the established standard for magnetite[35],which demonstrates a correlation between peak broadening in XRD and particle size.The average size of the crystallites in the magnetic Fe_3O_4-NPs of green synthesis was 7.72 nm.As a result, in an XRD examination, a peak with a greater intensity indicates a larger concentration of the mineral or molecule under study, as shown in Fig. 6 (A and B).

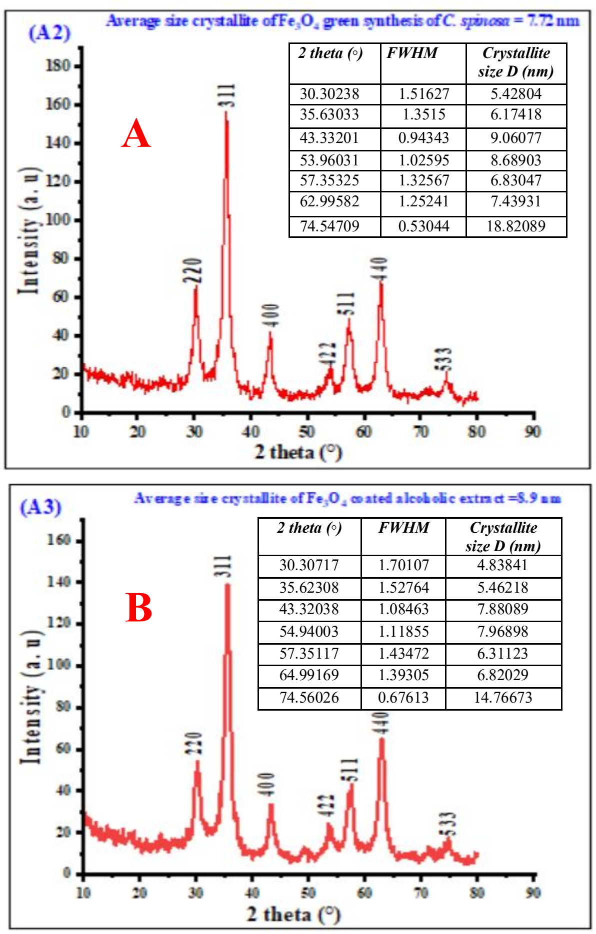

Figure 6. **XRD analysis results of (A) Fe_3O_4-NPs green synthesis from *C. spinosa* and (B) Fe_3O_4-NPs coated with alcoholic extract of *C. spinosa.***

Zeta Potential (ZP)

The speed at which charged particles move across the sample solution and towards the electrode in an electric field serves as a measure of the double layer's electrical potential (ZP). Most ZP readings are +/- 100 mV. ZP size predicts colloidal durability. ZP is stable at > +25 or <-25 mV NPs**.**The negative ZP of the particles serves as an illustration of this Fig. 7(a) ZP shows that the particles or colloids in Fe_3O_4 from *C. spinosa* have an average electric charge of -17.8 mV. It indicates thepotential for particle aggregation or dispersion. A negative ZP suggests that the particles tend to repel eachother, thereby promoting stability in the sample. The peak 1 value of -18.9 mV corresponds to a specific peak observed in the ZP distribution graph. This peak represents a higher frequency or concentration of particles with a ZP value of approximately -18.9 mV [36]. The size distribution of the particles of Fe_3O_4-coated alcoholic extracts of *C. spinosa* was examined.

The ZP was in the -25mV range in Fig. 7(b), indicating that the particles were stable. Because of the strong repelling interactions between the particles in the solution, this suggests that they have a high degree of stability. The particles are likely to have a negative charge, which helps avoid aggregation and guarantees uniform dispersion in the solution. This information helps us understand the overall charge characteristics of the particles or colloids in the sample. The particles probably have a negative charge, which prevents them from aggregating and ensures that they are evenly dispersed throughout the fluid. This is demonstrated by the fact that the particles have negative ZP values.

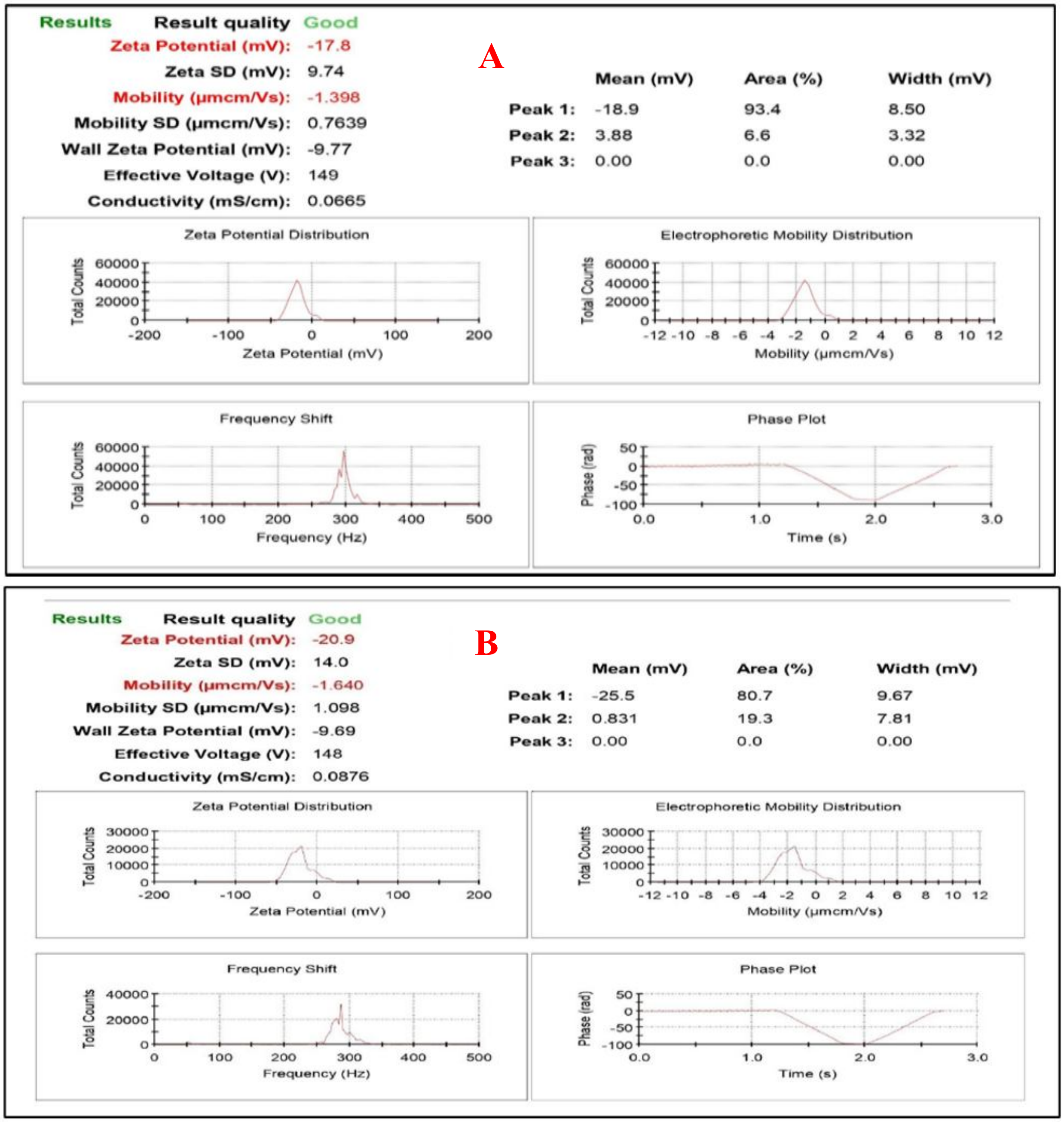

Figure 7. **Zeta Potential analysis results of (A) Fe_3O_4-NPs green synthesis from *C. spinosa* and (B) Fe_3O_4-NPs coated with alcoholic extract of *C. spinosa.***

Study of cancer cell line activity to determine the optimal IC_{50} concentration, using nanocomposites extracts

In this investigation, it was shown that nanocomposite extracts with an IC_{50} concentration of 1.25 µg/mL may help to stop colon cancer cell growth. Cell viability significantly decreased when the nanocomposite concentration was increased to 20 µg/mL, demonstrating a dose-dependent effect. When Fe_3O_4-NP green synthesis is used in different composites, such as Fe_3O_4-NPs only, Fe_3O_4-coated with crude *C. spinosa*, and Fe_3O_4-coated with alcoholic extract from *C. spinosa* are given in Table 4.

Table 4. **Samples used for the anticancer activity of Fe_3O_4-NP green synthesis in *C. spinosa.***

Codes	*Samples*
A	Iron oxide nanoparticles Fe_3O_4-NPs only
B	Fe_3O_4-coated crude of C. spinosa
C	Fe_3O_4-coated alcoholic extract of C. spinosa

The IC50 value was affected by human dermal fibroblast (HDF) cell lines used as representative healthy cell models.of healthy cells. By analysing the results, we compared the effects of nanocomposite extracts on HDF and HCT116 colon cancer cell lines. The IC_{50}value represents the concentration of the composite that inhibits 50% of cell viability. A lower IC_{50} value indicates that the composite is more cytotoxic to the cells.Based on the provided result for the HTC116 cells, which are a human colon cancer cell line, the IC_{50}values for samples A, B, and C were 78.95, 52.32, and 32.49 µg/mL, respectively (Fig. 8). This supports the IC_{50} values in cell viability studies. Chemicals inhibit cell growth or viability by 50% at IC_{50}. This inhibitory effect requires less material with a lower IC_{50}. Chemicals seem to suppress cancer cells better [37].

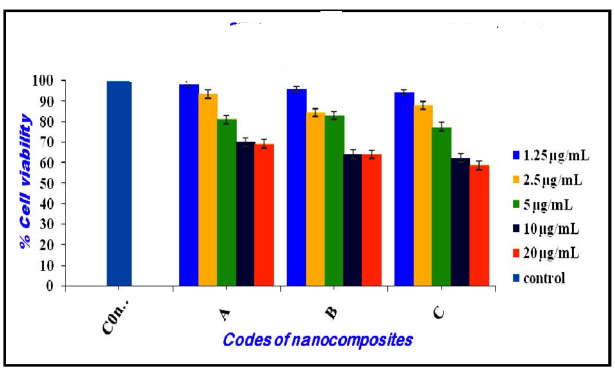

Figure 8. **The IC_{50} of (A) Fe_3O_4 (B), Fe_3O_4-coated crude of *C. spinosa* and (C) Fe_3O_4-NPs-coated with an alcoholic extract of *C. spinosa* for HCT-116**

However, the choice of the best IC_{50}value depends on the intended application of the composite and the type of cells being used. For example, if the goal is to develop a cancer treatment, a lower IC_{50} value may be desirable because it indicates that the composite is more effective at killing cancer cells.However, if the goal is to develop a material for tissue engineering, a higher IC_{50} value may be desirable because it indicates that the composite is less toxic to cells and may be more suitable for use in the body. The viability values for each sample were obtained at different concentrations of 1.25, 2.5, 5, 10, and 20 µg/mL of the composite and are presented as percentages. The highest average viability values for each sample (A, B, and C) were also calculated, with HTC 116 having the highest average viability for A (69.25± 1.07%), B (64.24±4.73%), and C (58.70±2.03%) at concentration 20 µg/mL, respectively as shown in Table 5 [38].

Table 5. **Result of HTC-116 anticancer activity in different concentrations of Fe_3O_4-NPs.**

Concentration (µg/mL)	A	B	C
Control/ 100	0	0	0
1.25	98.56	96.15	94.52
2.5	93.70	84.81	88.08
5	81.16	83.21	77.67
10	70.41	64.34	62.4
20	69.25	64.24	58.7
Value of IC_{50} µg/mL	78.95	52.32	32.49

Considering the results, green synthesis is achievable. This method prioritizes eco-friendly NPs like Fe_3O_4. It may not be against cancer as well as other methods, but it might help preserve sustainability. While less effective against cancer cells, Fe_3O_4-NPs may promote plant growth and have antifungal, antibacterial, and magnetic-hyperthermia uses [39].

The Fe_3O_4-NPs are enveloped with a diverse array of phytochemicals derived from *C. spinosa* by a method that uses unrefined *C. spinosa*. Identifying the specific active compounds and their distinct mechanisms of action is difficult, despite the presence of several bioactive components in crude extracts[40]. The alcoholic extract of *C.*

*spinosa*was used to increase the concentration of certain bioactive compounds obtained from theplant by applying it to Fe_3O_4. This methodhas the potential to provide a morefocused approach compared to unrefined extracts, thereby improving effectiveness. *C. spinosa* is well-known for its wide range of bioactive compounds, including alkaloids, flavonoids, steroids, terpenoids, and tocopherols [41]. On the other hand, HDF stands for Human Dermal Fibroblasts, which are normal healthy cells commonly used as controls in cancer cell experiments. The average viability A (71.70±0.32%), B (70.87±2.55%), and C (75.27±7.90%), with IC_{50} for these samples were (243.77, 488.23, and 569.47) µg/mL, respectively [38]. Fig. 9 represents the concentration of the composite required to inhibit the growth of 50% of the cells.

The viability values represent the percentage of cells that remained alive and healthy after exposure to the composite at different concentrations, as explained in Table 6. The ideal viability percentage for developing a cancer drug depends on the drug's specific requirements and the intended application. In some cases, a high viability percentage may be acceptable if the composite is intended to slow down the growth of cancer cells rather than kill them outright. In other cases, a low viability percentage may be desirable if the composite is intended to kill cancer cells more effectively. According to ISO 10993-5, a percentage of cell viability above 80% is considered non-cytotoxicity; within 80%–60% weak; 60%–40% moderate; and below 40% strong cytotoxicity, respectively[42].Therefore, the ideal IC_{50} and viability values depend on the cell line being tested. For cancer cells such as HTC 116, lower IC_{50} values and cell viability values would be desirable, whereas for normal cells such as HDF, higher IC_{50} values and higher viability values would be desirable.

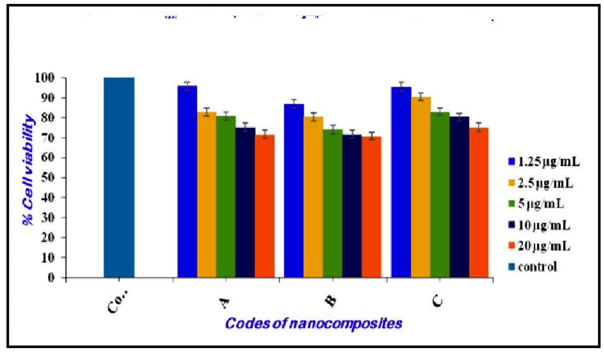

Figure 9.**The IC_{50} of (A) Fe_3O_4 (B), Fe_3O_4-coated crude of *C. spinosa* and (C) Fe_3O_4-NPs-coated with an alcoholic extract of *C. spinosa* for HDF**

Table 6. **Result of HDF anticancer activity in different concentrations of Fe_3O_4-NPs.**

Concentration (µg/mL)	*A*	*B*	*C*
Control/ 100	0	0	0
1.25	95.8	86.94	95.66
2.5	82.88	80.33	90.6
5	80.71	74.25	82.98
10	75.3	71.85	80.23
20	71.7	70.87	75.27
Value of IC_{50} µg/mL	243.77	488.23	569.47

Conclusion

This study reveals that green methods for synthesizing iron nanoparticles show stability and potential for use in medication delivery and environmental cleanup. The use of an alcoholic extract of *C. spinosa* as a covering agent can increase the production of these nanoparticles, making their production more sustainable. The shape and structure of the nanoparticles were characterized using TEM and FESEM, and zeta potential provided insights into their surface charges. FTIR and XRD analyses were used to analyze the functional groups and bonding of the nanoparticles. FESEM analysis revealed spherical and aggregated Fe_3O_4-NPs, while XRD analysis suggested pure, crystalline particles. The study also tested the potential toxicity of Fe_3O_4-NPs on HTC 116 cells, finding that the viability of these cells was only slightly different after 72 h compared to nanocomposites like Fe_3O_4-coated crude and coated with an alcoholic extract of *C. spinosa.*

Conflict of Interest

On behalf of all authors, the corresponding author states (MAJID) that there is no conflict of interest.

References

1 C. Lans, *J. Ethnopharmacol.*, 236 (2019) 366. https://doi.org/10.1016/j.jep.2019.02.030

2 M. K. Singh and O. S. Bindhu, *Plant latex: A Rich Source of Haemostatic Proteases*, (2019).143-153 p https://doi.org/10.1007/978-981-13-7248-3_10

3 E. Salmerón-Manzano, J. A. Garrido-Cardenas and F. Manzano-Agugliaro, *Int. J. Environ. Res. Public Health*,17 (2020) 10. https://doi.org/10.3390/ijerph17103376

4 M. J. R. Howes, C. L. Quave, J. Collemare, E. C. Tatsis, D. Twilley, E. Lulekal, A. Farlow, L. Li, M. E. Cazar, D. J. Leaman, T. A. K. Prescott, W. Milliken, C. Martin, M. N. De Canha, N. Lall, H. Qin, B. E. Walker, C. Vásquez-Londoño, B. Allkin, M. Rivers, M. S. J. Simmonds, E. Bell, A. Battison, J. Felix, F. Forest, C. Leon, C. Williams and E. Nic Lughadha, *Plants People Planet*, 2 (2020) 463. https://doi.org/10.1002/ppp3.10138

5 M. L. Foschi, M. Juan, B. Pascual and N. Pascual-Seva, *Agronomy*, 10 (202) 6. https://doi.org/10.3390/agronomy10060838

6 J. Jiménez-López, A. Ruiz-Medina, P. Ortega-Barrales and E. J. Llorent-Martínez, *Food Chem.*, 250 (2018) 54. https://doi.org/10.1016/j.foodchem.2018.01.010

7 X. Zhao, W. Liu, Z. Cai, B. Han, T. Qian and D. Zhao, *Water Res.*, 100 (2016) 245. https://doi.org/10.1016/j.watres.2016.05.019

8 S. Ying, Z. Guan, P. C. Ofoegbu, P. Clubb, C. Rico, F. He and J. Hong, *Environ. Technol. Innov.*, 26 (2022) 102336. https://doi.org/10.1016/j.eti.2022.102336

9 B. Ajitha, Y. Ashok Kumar Reddy and P. S. Reddy, *Spectrochim. Acta - Part A Mol. Biomol. Spectrosc.*, 121 (2014) 164. https://doi.org/10.1016/j.saa.2013.10.077

10 S. Nayak, S. P. Sajankila, C. V. Rao, A. R. Hegde and S. Mutalik, *Energ. Sources, Part A Recover. Util. Environ. Eff.*, 43 (2021) 3415. https://doi.org/10.1080/15567036.2019.1632394

11 M. Shah, D. Fawcett, S. Sharma, S. K. Tripathy and G. E. J. Poinern, *Green Synthesis of Metallic Nanoparticles Via biological Entities*, 8 (2015) 7278. https://doi.org/10.3390/ma8115377

12 L. Castro, M. L. Blázquez, J. A. Muñoz, F. González, C. García-Balboa and A. Ballester, *Process Biochem.*, 46 (2011), 1076. https://doi.org/10.1016/j.procbio.2011.01.025

13 J. K. Patra and K. H. Baek, *J. Nanomater.* 2014 (2014) 12. https://doi.org/10.1155/2014/417305

14 M. S. Akhtar, M. K. Swamy and U. R. Sinniah, *Natural Bio-active Compounds. Vol. 1 Production and Application*, (2019) 1. https://doi.org/10.1007/978-981-13-7154-7

15 I. Ali, *Curr. Cancer Drug Targets*, 11 (2011) 131. doi:10.2174/156800911794328457

16 A. You, M. A. Y. Be and I. In,.2475 (2023) 040010-1- 040010-9 https://doi.org/10.1063/5.0103401

17 X. Zhou, J. Peng, G. Fan and Y. Wu, *J.*

Chromatogr. A, 1092 (2005) 216. https://doi.org/10.1016/j.chroma.2005.07.064

18 Z. Wang, J. Guo, J. Ma and L. Shao, *J. Mater. Chem. A*, 3 (2015) 19960. doi:https://doi.org/10.1039/C5TA04840K

19 A. Alangari, M. S. Alqahtani, A. Mateen, M. A. Kalam, A. Alshememry, R. Ali, M. Kazi, K. M. Alghamdi and R. Syed, *Adsorpt. Sci. Technol.*, 2022, (2022) 9 https://doi.org/10.1155/2022/1562051

20 S. Kanagasubbulakshmi and K. Kadirvelu, *Def. Life Sci. J.*, 2 (2017) 422. https://doi.org/10.14429/dlsj.2.12277

21 A. J. Shnoudeh, I. Hamad, R. W. Abdo, L. Qadumii, A. Y. Jaber, H. S. Surchi and S. Z. Alkelany, *Synthesis, Characterization, and Applications of Metal Nanoparticles*, Elsevier Inc., (2019). https://doi.org/10.1016/B978-0-12-814427-5.00015-9

22 L. Nalbandian, E. Patrikiadou, V. Zaspalis, A. Patrikidou, E. Hatzidaki and C. N. Papandreou, *Curr. Nanosci.*, 12 (2015) 455. doi:10.2174/1573413712666151210230002

23 F. Fajaroh, H. Setyawan, W. Widiyastuti and S. Winardi, *Adv. Powder Technol.*, 23 (2012) 328. https://doi.org/10.1016/j.apt.2011.04.007

24 S. J. Hoseini, H. Nasrabadi, M. Azizi, A. S. Beni and R. Khalifeh, *ChemInform*,43 (2013) 1683-1691 p https://doi.org/10.1080/00397911.2012.663048

25 A. Demir, R. Topkaya and A. Baykal, *Polyhedron*, 65 (2013) 282. https://doi.org/10.1016/j.poly.2013.08.041

26 K. Yang, H. Peng, Y. Wen and N. Li, *Appl. Surf. Sci.*, 256 (2010) 3093. https://doi.org/10.1016/j.apsusc.2009.11.079

27 M. Mahdavi, F. Namvar, M. Bin Ahmad and R. Mohamad, *Molecules*,18 (2013) 5954. https://doi.org/10.3390/molecules18055954

28 S. S. Alterary and A. Alkhamees, *Green Process. Synth.*, 10 (2021) 384. https://doi.org/10.1515/gps-2021-0031

29 M. M. Ba-Abbad, A. Benamour, D. Ewis, A. W. Mohammad and E. Mahmoudi, *Jom*.74 (2022) 3531. https://doi.org/10.1007/s11837-022-05380-3

30 M. Bagtash, Y. Yamini, E. Tahmasebi, J. Zolgharnein and Z. Dalirnasab, *Microchim. Acta*, 183 (2016) 449. doi:10.1007/s00604-015-1667-5

31 Q. Wang, S. Snyder, J. Kim and H. Choi, *Environ. Sci. Technol.*, 43 (2009) 3292. doi:10.1021/es803540b

32 J. B. Fathima, A. Pugazhendhi, M. Oves and R. Venis, *J. Mol. Liq.*, 260 (2018) 1. https://doi.org/10.1016/j.molliq.2018.03.033

33 S. Khodabakhshi, B. Karami, K. Eskandari, S. J. Hoseini and H. Nasrabadi, *Arab. J. Chem.*, 10 (2017) S3907. https://doi.org/10.1016/j.arabjc.2014.05.030

34 H. Shagholani, S. M. Ghoreishi and M. Mousazadeh, *Int. J. Biol. Macromol.*, 78 (2015) 130. https://doi.org/10.1016/j.ijbiomac.2015.02.042

35 M. Mahdavi, M. Bin Ahmad, M. J. Haron, Y. Gharayebi, K. Shameli and B. Nadi, *J. Inorg. Organomet. Polym. Mater.*, 23 (2013) 599. https://doi.org/10.1007/s10904-013-9820-2

36 M. Kędzierska, P. Potemski, A. Drabczyk, S. Kudłacik-Kramarczyk, M.

Głab, B. Grabowska, D. Mierzwiński and B. Tyliszczak, *Molecules*, 26 (2021) 1744 doi:10.3390/molecules26061744

37 A. Pakdemirli, C. Karaca, T. Sever, E. Daskin, A. Leblebici, T. Yiğitbaşi and Y. Başbinar, *Turk. J. Med. Sci.*, 50 (2020) 271. doi:10.3906/sag-1907-173

38 A. G. Quiroga, M. Cama, N. Pajuelo-Lozano, A. Álvarez-Valdés and I. S. Perez, *ACS Omega*, 4 (2019) 21855. doi:10.1021/acsomega.9b02831

39 L. Alili, S. Chapiro, G. U. Marten, A. M. Schmidt, K. Zanger and P. Brenneisen, *Biomed Res. Int.*, 2015 (2015) 1. https://doi.org/10.1155/2015/530957

40 A. M. Alkhaibari and A. D. Alanazi, *Evidence-based Complement. Altern. Med.*, 2022 (2022) https://doi.org/10.1155/2022/6371274

41 H. Zhang and Z. F. Ma, *Nutrients*, 10 (2018) 1. https://doi.org/10.3390/nu10020116

42 J. López-García, M. Lehocký, P. Humpolíček and P. Sáha, *J. Funct. Biomater.*, 5 (2014) 43. https://doi.org/10.3390/jfb5020043